arXiv:1109.2668v1 [astro-ph.EP] 13 Sep 2011

Climate instability on tidally locked exoplanets

Edwin S. Kite

Department of Earth and Planetary Science, University of California at Berkeley, CA 94720

Center for Integrative Planetary Science, University of California at Berkeley, CA 94720

kite@berkeley.edu

Eric Gaidos

Department of Geology and Geophysics, University of Hawaii at Manoa, Honolulu, HI 96822

Michael Manga

Department of Earth and Planetary Science, University of California at Berkeley, CA 94720

Center for Integrative Planetary Science, University of California at Berkeley, CA 94720

ABSTRACT

Feedbacks that can destabilize the climates of synchronously-rotating rocky planets may arise on planets with strong day-night surface temperature contrasts. Earth-like habitable planets maintain stable surface liquid water over geological time. This requires equilibrium between the temperature-dependent rate of greenhouse-gas consumption by weathering, and greenhouse-gas resupply by other processes. Detected small-radius exoplanets, and anticipated M-dwarf habitable-zone rocky planets, are expected to be in synchronous rotation (tidally locked). In this paper we investigate two hypothetical feedbacks that can destabilize climate on planets in synchronous rotation. (1) If small changes in pressure alter the temperature distribution across a planet's surface such that the weathering rate goes up when the pressure goes down, a runaway positive feedback occurs involving increasing weathering rate near the substellar point, decreasing pressure, and increasing substellar surface temperature. We call this feedback *enhanced substellar weathering instability* (ESWI). (2) When decreases in pressure increase the fraction of surface area above the melting point (through reduced advective cooling of the substellar point), and the corresponding increase in volume of liquid causes net dissolution of the atmosphere, a further decrease in pressure will occur. This *substellar dissolution feedback* (SDF) can also cause a runaway climate shift. We use an idealized energy balance model to map out the conditions under which these instabilities may occur. In this simplified model, the weathering runaway can shrink the habitable zone, and cause geologically rapid 10^3-fold atmospheric pressure shifts within the habitable zone. Mars may have undergone a weathering runaway in the past. Substellar dissolution is usually a negative feedback or weak positive feedback on changes in atmospheric

pressure. It can only cause runaway changes for small, deep oceans and highly soluble atmospheric gases. Both instabilities are suppressed if the atmosphere has a high radiative efficiency. Our results are most relevant for atmospheres that are thin, have low greenhouse-gas radiative efficiency, and have a principal greenhouse gas that is also the main constituent of the atmosphere. These results identify a new pathway by which habitable-zone planets can undergo rapid climate shifts and become uninhabitable.

Subject headings: planetary systems – planets and satellites: general– stars: individual(Kepler-10, CoRoT-7, GJ1214, 55 Cnc, Kepler-9, Kepler-11)

1. Introduction

Exoplanet research is driven in part by the hope of finding habitable planets beyond Earth (Exoplanet Community Report 2009). Demonstrably habitable exoplanets maintain surface liquid water over geological time. Earth's long-term climate stability is believed to be maintained by a negative feedback between control of surface temperature by partial pressure of CO_2 (pCO_2), and temperature-dependent mineral weathering reactions that reduce pCO_2 (Walker et al. 1981). There is increasing evidence that this mechanism does, in fact, operate on Earth (Cohen et al. (2004),Zeebe & Caldeira (2008), but see also Edmond & Huh (2003)). The Circumstellar Habitable Zone hypothesis (Kasting et al. 1993) extends this stabilizing feedback to rocky planets in general, between top-of-atmosphere flux limits set by the runaway greenhouse (upper limit) and condensation of thick CO_2 atmospheres (lower limit). H_2-H_2 collision-induced opacity can extend the habitable zone further out, in theory (Pierrehumbert & Gaidos 2011; Wordsworth 2011). Currently the best prospects for finding stable surface liquid water orbit M stars (Tarter et al. 2007; Deming & Seager 2009). Planets in M-dwarf habitable zones are close enough to their star for tidal despinning and synchronous rotation (Murray & Dermott (1999), Chapter 5). Nearby M-dwarfs are the targets of several ongoing and proposed planet searches. Rocky exoplanets in hot orbits have recently been confirmed (Léger et al. 2011; Batalha et al. 2011; Winn et al. 2011), and are presumably in synchronous rotation. But does the habitable zone concept hold water for tidally locked planets?

In this paper, we highlight two closely-related feedbacks which could cause climate destabilization on planets with and low-opacity atmospheres and atmospheres that do not have large optical depth. Both feedbacks require surface temperatures near the substellar point to be significantly higher than the planet-average surface temperature.

- The *enhanced substellar weathering instability* (ESWI) flows out of the same strong temperature dependence of silicate weathering that makes it possible for carbonate-silicate feedback to stabilize Earth's climate (Walker et al. 1981). Weathering and hence CO_2 drawdown rate increases rapidly with increasing temperature. Weathering also increases with rainfall, which

increases with temperature (O'Gorman & Schneider 2008; Pierrehumbert 2002; Schneider et al. 2010). Therefore, the global CO_2 loss rate depends heavily on the maximum temperature. On a synchronously-rotating planet where ΔT_s is high, most of the weathering occurs near the substellar point. Suppose weathering is initially adjusted to match net supply of greenhouse gases by other processes (e.g., volcanic degassing). Then consider a small increase in atmospheric pressure. Average temperature must increase, unless there is an antigreenhouse effect. Normally, this would lead to an increase in weathering. However, on a planet with a strong day-night temperature contrast, most of the weathering occurs near the substellar point. An increase in atmospheric pressure can decrease temperature around the substellar point, if increased advection of heat away from the hotspot by winds outweighs any increase in greenhouse forcing. Because this substellar area is cooling, and most of the weathering is around the substellar point, the planet-averaged weathering rate declines. Volcanic supply of greenhouse gases now outpaces removal by weathering, and a further increase in pressure occurs. This instability can lead to very strong greenhouse forcing, and may trigger a moist runaway greenhouse (Kasting 1988). Conversely, a small decrease in pressure from the unstable equilibrium can lead to atmospheric collapse. ESWI requires that weathering is an important sink for the major climate-controlling greenhouse gas, which is also the dominant atmospheric constituent. It also requires that the atmosphere is important in setting the mean surface temperature.

- *Substellar dissolution feedback* (SDF) supposes an increasing gradient in surface temperature on an initially frozen planet, which allows a liquid phase to form (or be uncovered) around the substellar point. Some atmosphere dissolves in the new liquid phase. Positive feedback is possible if the decrease in atmospheric pressure due to dissolution raises the temperature around the substellar point, increasing the fraction of the planet's surface area above the melting point. (We assume for the moment that P exceeds the triple point). In order for the mass of atmosphere sequestered in the pond to increase with decreasing pressure, increasing pond volume must outcompete both Henry's-law decrease in gas dissolved per unit volume, and the decrease in gas solubility with increasing temperature. For example, suppose $c \propto P$, where c is the concentration of gas in the pond and P is the atmospheric pressure, and $V \propto P^{-n}$ with V the ocean volume. Then $n > 1$ is sufficient for positive feedback, and $n > 2$ is sufficient for runaway. So long as the runaway condition is satisfied, the area of liquid stability will continue to expand: a pond becomes an ocean, drawing down the atmosphere. As with the ESWI, the key is that substellar temperature increases as pressure decreases. Runaway SDF implies a climate bistability for a given inventory of volatile substance. One equilibrium has all of the volatile in the atmosphere. The other equilibrium has most of the volatile substance sequestered in a regional ocean and a little in the atmosphere, with the ocean prevented from completely freezing over by the steep temperature gradient that the thin atmosphere enables. A similar hysteresis was proposed for ancient Titan by Lorenz et al. (1997). Runaway SDF is separate from the feedback between retreating ice cover and increased absorption of sunlight (ice-albedo feedback; Roe & Baker (2010)), although both

are likely to operate together.

Both instabilities occur more slowly than thermal equilibration of the atmosphere and surface. This separation of timescales allows us to solve for the fast processes that set the surface temperature (in §2), and then separately address each of the two slower processes which may cause atmospheric pressure to change (in §3-§4).

Day-night color temperature contrast is among the 'easiest' parameters to be measured for a transiting exoplanet (Cowan & Agol 2011), but there is currently no theory for ΔT_s on planets with observable surfaces. One motivation for this paper is to contribute to this emerging theory. We use a simplified approach which complements more sophisticated exoplanet Global Circulation Models (GCMs) (Joshi et al. 1997; Joshi 2003; Merlis & Schneider 2010; Edson et al. 2011; Wordsworth et al. 2011; Pierrehumbert 2011). §2 sets out the energy balance model that is used for both instabilities, and §3 explains the enhanced substellar weathering instability including our choice of weathering parameterization. §4 explains the substellar dissolution feedback (considering only the 1:1 spin-orbit resonance). We find that SDF doesn't work in most cases, so readers motivated by short-term detectability can safely omit §4 and move to §5. §5.1 discusses relevant solar system data, including the possibility that Mars underwent a form of ESWI. §5.2 discusses applicability to exoplanets, and §6 summarizes results.

2. Idealized energy balance model

Consider a planet in synchronous rotation on which surface liquid water is stable, with an atmospheric temperature that decreases with height along the dry adiabat. Slow rotation weakens the Coriolis effect, allowing the atmospheric circulation to all but eliminate horizontal gradients in atmospheric temperature at the top of the boundary layer, T_a. This is the weak temperature gradient approximation often made for Earth's tropics (e.g. Merlis & Schneider (2010)). Figure 1 shows the setup for our idealized energy balance model. The surface temperature $T_s(\psi)$ at an angular separation ψ from the substellar point is set by the local surface energy balance:-

$$SW_s(\psi) - LW\uparrow(\psi) + LW\downarrow - \beta(T_s(\psi) - T_a) = 0 \tag{1}$$

where $SW_s(\psi)$ is starlight absorbed by the surface, $LW\uparrow(\psi) = \eta\sigma T_s(\psi)^4$ (where σ is the Stefan-Boltzmann constant and $\eta \approx 1.0$ is the emissivity at thermal wavelengths) is the surface thermal radiation, $LW\downarrow$ is backradiation from the atmosphere, β is a turbulent heat transfer coefficient ($\beta = k_{TF}\ \rho$, where ρ is the near-surface atmospheric density divided by Earth's sea-level atmospheric density, and k_{TF} is a turbulent flux proportionality constant), and T_a is the temperature of the atmosphere at the top of the boundary layer. (Equatorial superrotating jets can cause the hottest point on the surface to be downwind from the substellar point (Knutson et al. 2009; Mitchell & Vallis 2010; Liu & Schneider 2011)). The shortwave flux $SW_s(\psi) = L_*(1-\alpha)\cos(\psi)$ corresponds

to stellar flux L_*, attenuated by surface albedo α. There is negligible transport of heat below the surface: we assume seas are not globally interconnected (or are shallow, or are deeply buried, or do not exist) and energy flux from the interior is small.

$LW\downarrow$ ($= \frac{1}{2}\int_0^\pi LW\uparrow(\psi)\,\sin\psi\,\mathrm{d}\psi - OLR$, ignoring turbulent fluxes) is longwave flux from the atmosphere to the surface. OLR (Outgoing Longwave Radiation, longwave energy exiting the top of the atmosphere) is given by interpolation in a look-up table. To build this look-up table, we slightly modified R.T. Pierrehumbert's scripts at `http://geosci.uchicago.edu/~rtp1/Principles PlanetaryClimate/`, particularly `PureCO2LR.py`. The look-up table gives $OLR(P_\Lambda, T_s)$ for a pure noncondensing CO_2 atmosphere on the dry adiabat, with the temperature at the bottom of the adiabat equal to the energy-weighted average T_s, and with Earth gravity (9.8 m/s^2). Our noncondensing assumption introduces large errors for $T_s < 175$K, so we assume that the top-of-atmosphere effective emissivity $OLR/LW\uparrow$ at these low temperatures is the same as at $T_s = 175$K.

To investigate atmospheres not made of pure CO_2, we introduce an opacity ratio or relative radiative efficiency Λ, which is the ratio of the radiative efficiency of the atmosphere of interest to that of pure noncondensing CO_2. Λ is a simplification of the complicated behavior of real gas mixtures (Pierrehumbert 2010). Λ can be greater than 1 if the atmosphere contains radiatively very efficient gases (chloroflourocarbons, CH_4, NH_3, or the "terraforming gases"; Marinova et al. (2005)). We then query the look-up table using $P_\Lambda = \Lambda P$. Smaller values of Λ have a weaker greenhouse effect (increased OLR).

Rayleigh scattering is relatively unimportant for planets orbiting M-dwarfs. Starlight is concentrated at red wavelengths where Rayleigh scattering is ineffective (falling off as λ^{-4}, where λ is wavelength). The optical depth to Rayleigh scattering of 1 bar of Earth air is 0.16 for light from the Sun, but only 0.02 for light from the Super-Earth hosting M3 dwarf Gliese 581 (approximating both stars as blackbodies). In addition, absorption of starlight by the atmosphere is much stronger in the NIR than the visible, and so is more effective at compensating for Rayleigh scattering as star temperature decreases (Pierrehumbert 2010). We neglect Rayleigh scattering and absorption of starlight by the atmosphere.

The horizontally uniform atmospheric boundary layer temperature, T_a, is set by the total energy balance of the atmosphere,

$$\frac{1}{2}\int_0^\pi [LW\uparrow(\psi) + \beta(T_s(\psi) - T_a)]\,\sin\psi\,\mathrm{d}\psi - OLR - LW\downarrow = 0 \tag{2}$$

where the integral gives the average flux from the surface. This reduces to $T_a = {}^1\!/_2 \int_0^\pi T_s(\psi)\,\sin\psi\,\mathrm{d}\psi$ because of our particular choice of $LW\downarrow$. In effect, we assume that the boundary layer only interacts with the ground through turbulent fluxes.

For a given P_Λ, we iterate to find T_a and $T_s(\psi)$. ψ resolution is 5 degrees. The initial condition has the surface in radiative equilibrium, and the atmosphere in equilibrium with this

surface temperature distribution. Convergence tolerance is $\approx 2 \times 10^{-6}$.

Throughout the paper, we assume $k_{TF} = C_p(T_a)C_D U$, where $C_p(T_a)$ is the temperature-dependent specific heat capacity of CO_2 ($\approx$850 J/kg/K at 300K), C_D is a drag coefficient, and U is characteristic near-surface wind speed. $C_D = \frac{k_{VK}^2}{\ln(z_1/z_0)^2}$ where $k_{VK} = 0.4$ is von Karman's constant, $z_1 = 10$m is a reference altitude, and z_0 is the surface roughness length (10^{-4} m, which is bracketed by the measured values for sand, snow, and smooth mud flats; Pielke (2002)). For our reference $U = 10$ m/s, this gives $k_{TF}\,\rho = 12.3$ W/m^2/K. We assume a Prandtl number near unity. §5.2.1 reports sensitivity tests using different values of U.

We accept the following inconsistencies to reduce the complexity of the model:- (1) Radiative disequilibrium drives T_s to a higher value than T_a at the surface, and turbulence can never completely remove this difference. Therefore, setting the temperature at the bottom of the atmosphere to the surface temperature will lead to an overestimate of $LW\downarrow$ at low P. (2) The expression for k_{TF} is appropriate for a neutrally stable atmospheric surface layer, but turbulent mixing is inhibited on the nightside by a thermal inversion (Merlis & Schneider 2010). This will tend to make the coupling between nightside atmosphere and nightside surface too strong. (3) We assume an all-troposphere atmosphere with horizontally uniform temperature. Merlis & Schneider (2010) find temperatures are nearly horizontally uniform for Earthlike surface pressure and for levels in the atmosphere at pressures less than half the surface pressure. Atmospheric temperature is approximately horizontally uniform when the transit time for a parcel of gas across the nightside, $\tau_{advect} = \frac{a}{U_h}$, is short compared to the nightside radiative timescale, $\tau_{rad} \sim \frac{P}{g}\frac{C_p}{4\epsilon\sigma T^3}$ (Showman et al. 2010). Here, a is planet radius (1 Earth radius), U_h is high-altitude wind speed ($\sim$ 30 m/s: Merlis & Schneider (2010)), ϵ is an greenhouse parameter corresponding to the fraction of the emitted radiation that is not absorbed by the upper atmosphere and escapes to space, and $T = 250$K is the atmospheric temperature, the radiative equilbrium temperature on the darkside being zero. Picking $\epsilon = 0.5$, this gives $\tau_{advect} \sim 2$ days and $\tau_{rad} \sim 50$ days. (4) The treatment of T_a is crude. (5) We assume the atmosphere is transparent to stellar radiation, which is a crude approximation under M-dwarf (or cloudy) skies. (6) We neglect condensation within the atmosphere.

Representative temperature plots are shown in Figure 2, for $\Lambda = 0.1$ and $L_* = 900$ W/m^2. At low pressures, nightside temperatures are close to absolute zero, and substellar temperature is close to radiative equilibrium. Increasing pressure cools $\psi < 60°$, and warms $\psi > 70°$. This is beause the atmosphere is warmer than the surface on the nightside, and cooler than the surface on the dayside. Therefore, the increase in $P(\propto \beta)$ increases the $\beta(T_s - T_a)$ term, which warms the nightside, but cools the dayside. For positive Λ, $LW\downarrow$ will increase with P and warm the entire planet. However, for the relatively small value of Λ shown here, the substellar point still undergoes net cooling with increasing pressure. This cooling with increasing P is what makes the ESWI and SDF possible. When the surface becomes nearly isothermal, as for the "10-bar" curve in Figure 2, the entire surface warms with increasing pressure, and the ESWI and SDF cannot occur.

For $\Lambda \geq 0$, $\bar{T_s}$ must increase with P. Even if there is no greenhouse effect, the homogenization

of the atmosphere will warm the planet on average because of the nonlinear dependence of T on energy input (Edson et al. 2011). For small optical depth, nightside $T_s \propto \ln(P)$. The fractional area of the planet over which liquid water is stable is 27% at radiative equilibrium, decreasing with pressure and vanishing at ∼0.7 bars. As P increases the greenhouse effect further, liquid stability reappears at ∼2.4 bars, rapidly becoming global.

3. Climate destabilization mechanism #1: Enhanced substellar weathering instability (ESWI)

3.1. Weathering parameterisation

.

The Berner & Kothavala (2001) weathering relation, which is specific to CO_2 weathering of Ca-Mg silicate rocks, states

$$\frac{W_\psi}{W_0} = \left(\frac{P}{P_0}\right)^{0.5} \underbrace{\exp\left[k_{ACT}\ (T_s(\psi) - T_o)\right]}_{\text{direct T dependence}} \underbrace{\left[1 + k_{RUN}\ (T_s(\psi) - T_o)\right]^{0.65}}_{\text{hydrology dependence}} \tag{3}$$

where W_ψ is local weathering rate, W_0 is a reference weathering rate, P is atmospheric pressure, P_0 is a reference pressure, $T_o = 273$K is a reference temperature, $k_{ACT} = 0.09$ is an activation energy coefficient, and k_{RUN} is a temperature-runoff coefficient fit to Earth GCMs. Equation 3 is widely used, but uncertain and controversial (§5.2.1). In our model, the strong temperature dependence leads to a strong concentration of weathering near the substellar point. For example, for a 1-bar atmosphere with $\Lambda = 0.1$ (shown in Figure 2), 93% of the weathering occurs in 10% of the planet's area. The planet-averaged weathering rate is

$$W_t(P) = \frac{1}{4\pi} \int_0^\pi W_\psi A_\psi \, \mathrm{d}\psi \tag{4}$$

Climate is in equilibrium ($\frac{\partial P}{\partial t} = 0$) when planet-integrated weathering of greenhouse gases, W_t, is equal to net supply V_n by other processes. The climate equilibrium is stable if $\mathrm{d}W_t/\mathrm{d}P > 0$ – in this case, carbonate-silicate feedback enables long-term climate stability (Walker et al. 1981). Climate destabilization occurs when $\mathrm{d}W_t/\mathrm{d}P < 0$. The weathering feedback that underpins the Circumstellar Habitable Zone concept (Kasting et al. 1993) changes sign, and acts to destabilize these climates.

3.2. ESWI results

Figure 3 shows weathering rates corresponding to the temperatures in Figure 2. The lines show equilibria between weathering consumption of greenhouse gases and net supply by other processes (Figure 3). The units of weathering are normalized to the weathering rate at $P = 3$ mbar. Along the curves, planet-integrated weathering of greenhouse gases, W_t, is equal to net supply V_n by other processes. These other processes can include volcanic degassing, metamorphic release, biology, sediment dissolution, and loss to space. The shape of this curve is set by competition between three effects:- (1) the greenhouse effect (Λ), (2) advective heat transport (β, k_{TF}) which enlarges and maintains unstable regions, and (3) stellar flux (L_*), which shrinks the unstable region. The curve has two stable branches and an unstable branch. The slope of the low-pressure stable branch is set by the (P/P_o) term in Equation 5 - for small P, $\tau \propto \ln(P)$ and $\beta \propto P$ are small and the atmosphere has little effect on T_s. On the intermediate pressure unstable branch – dashed in Figure 2 – the atmosphere is important to energy balance but β outcompetes τ. The homogenizing effect of β cools the substellar region, and planet-integrated weathering decreases with increasing pressure. In the high-pressure stable branch, the planet is close to isothermal. Further increases in β have little effect on ΔT_s, but τ warms the whole planet and now is able to increase W_t. Catastrophic jumps in the pressure caused by small changes in the supply V_n occur at ∼0.05 bar (for increasing volcanic activity) and ∼1 bars (for decreasing volcanic activity). The jumps correspond to a $>10^2$-fold increase in pressure, or a $>10^3$-fold decrease in pressure, respectively. The existence and location of these bifurcations are sensitive to small changes in the coefficients of (3). The timescale for the climate regime jump is set by the rate of weathering and/or rate of volcanism on each specific planet. For example, Earth today supplies ∼15 mbar CO_2 in 10^5 yr (atmosphere + ocean: linearizing, ∼2 x 10^7 yr to build up 1 bar CO_2), but an Io-like rate of resurfacing (Rathbun et al. 2004) with the same magmatic volatile content would build up 1 bar in $\sim O(10^{4-5})$ yr. A natural weathering-rate experiment occurred on Earth 0.054 Gya, with very rapid release of CO_2 from an unknown source. The warmed climate required $\Delta t \sim O(10^5)$ yr (Murphy et al. (2010), using ^{3}He accumulation dating) to draw down 0.9 mbar of excess CO_2 (Zeebe et al. 2009).

Figure 4 shows habitable-zone climate regimes as a function of equilibrium pressure and stellar flux, which can change (Figure 4a) due to stellar evolution, tidal migration (Jackson et al. 2010), or close encounters with other planets and small bodies (Morbidelli et al. 2007). Climate stability depends strongly on Λ, so we show this for three values of Λ - an almost radiatively inert gas (Figure 4b), an intermediate $\Lambda = 0.1$ case (Figure 4c), and a strong opacity that only just allows the ESWI (Figure 4d, for $\Lambda = 1.0$; higher values are stable against ESWI). The thick black line labelled with zeros corresponds to marginally stable climate equilibrium. Increasing L_* widens the range of P that sits within the low-pressure stable branch. That is because higher L_* produces higher absolute temperatures, and higher absolute temperatures favor radiative exchange between atmosphere and surface ($\propto 4(T_s - T_a)^3$ for small $(T_s - T_a)$) versus turbulent exchange ($\propto (T_s - T_a)^1$). Therefore, a given equilibrium value of P on the low pressure branch is more stable at low L_* than high L_* :– for a small increase in P the radiative warming will be less counteracted by the cooling of the substellar

point. Increasing L_* pushes the the high pressure branch to higher values. Other instabilities that contain the habitable zone are shown by thin lines. The dash-dotted line corresponds to pressures in excess of the nightside CO_2 saturation vapor pressure. CO_2 atmospheres to the left of this line condense on fast, dynamical timescales. Increasing Λ couples the horizontally-isothermal atmosphere more strongly to the nightside surface, and causes the CO_2 collapse threshhold to move to the left. The thin solid line corresponds to mean surface temperatures above 40°C, which is the lower edge of the moist runaway greenhouse zone (Kasting 1988; Pierrehumbert 1995) - our model does not include fluxes of latent heat or the greenhouse effect of water vapor, so the position of this line is notional. The maximum pressure and minimum pressure of the bifurcation loop (Figure 3) are shown by thick gray lines in figure 4. In some cases, the lower end-of-transition pressures are so low that water boils (thin dashed line). This would initiate the boiling of a global ocean. If boiling continued, the eventual fate could be a steam ocean, or restriction of liquid water stability to a thin belt near the terminator. The upper end-of-transition pressures are often >10 bars, with a nearly isothermal T_s. Such planets would have weak and perhaps undetectable phase curves in the absorbing bands (Selsis et al. 2011).

For the almost radiatively inert gas (Figure 4b), geologically stable equilibria usually have P <0.01 bars or P >0.3 bar. Intermediate pressures cannot be stable over geological time. The overall pattern is similar for $\Lambda = 0.3$ (Figure 4c). Increasing Λ always shrinks the domain of the unstable branch. For much higher Λ the climate is stable everywhere. We show the last gasp of the instability in Figure 4d. Higher radiative efficiency means that for a small change in P, when ΔT_s is significant, radiative heat transfer overcomes advective heat transfer, the substellar patch warms, and overall planet temperature increases.

Figure 5 summarizes the effects of ESWI in a stability phase diagram (against axes of gas radiative efficiency and incident stellar radiation). For $\Lambda > \sim 1$, the climate is stable to ESWI. For $\Lambda < \sim 1$, ESWI is possible but the pressure jumps caused by ESWI do not always have a catastrophic effect. Higher L_* warms the climate towards the runaway moist greenhouse threshhold, and upward jumps in pressure for $L_* > \sim 2000$ W m^{-2} may initiate the moist runaway greenhouse (points to the right of the vertical dashed line in Figure 5). Atmospheric collapse to $\sim$ 1 mbar (well below the triple point of water) only occurs below $\Lambda < 0.4$. Increasing L_* increases both the bottom and the top pressure for instability, implying that tidal migration towards the star should be destabilizing for thick atmospheres but stabilizing for thin atmospheres.

4. Climate destabilization mechanism #2: Substellar dissolution feedback (SDF)

Water ice and basalt are the most common planetary surface materials in the Solar System, and are expected to be common elsewhere.When these melt (around 273K for ice and 1300K for basalt), atmosphere can dissolve into the melt. Counterintuitively, a decrease in P and in average surface temperature $\bar{T}_s$ can favor melting if ΔT_s is large, as pointed out for Mars by Richardson & Mischna (2005). For a synchronously-rotating planet entirely coated in condensed material (ice, rock, or

carbon-rich ceramic), surface liquid will first appear near the substellar point. Atmosphere will dissolve into this warm little pond, approaching Henry's-law equilibrium:

$$P_{pond} = \frac{g}{P_{Earth}} \underbrace{\left(D_{pond} \frac{1}{2} \left(1 - \cos \psi_{max}\right) \right)}_{\text{global-equivalent liquid depth}} \underbrace{\left(P^d \, m \, \rho_l \, k_H(T^o) \exp\left[C \left(\frac{1}{T_{pond}} - \frac{1}{T^o} \right) \right] \right)}_{\text{mass of gas per unit liquid volume}} \quad (5)$$

where P_{pond} (in bars) is the equivalent atmospheric pressure of gases dissolved in the ocean, g is surface gravity, P_{Earth} = 1.01 x 10^5 Pa is a normalization constant, D_{pond} is pond depth, ρ_l is liquid density, ψ_{max} is the angular radius of the pond, P is the surface pressure, d is a dissolution exponent ($\sim$0.5 for water in silicate liquids and $\sim$1 for gases in water), m is the molecular mass of the atmosphere, k_H and C are Henry's-law coefficients, T_{pond} is the pond temperature, and T^o is a reference temperature. Here, the first term in brackets is the depth of the pond in global-equivalent meters, and the second term in brackets is the mass of gas per unit volume of pond. We have neglected the distinction between fugacity and partial pressure. The pond is assumed to be well-mixed so that $T_{pond} = \frac{1}{1-\cos\psi_{max}} \int_0^{\psi_{max}} T_{s,\psi} \sin\psi \, \mathrm{d}\psi$. This relation assumes a uniform heat transfer coefficient between the surface and the pond.

Instability occurs when a decrease (increase) in surface pressure results in an uptake (release) of gases from the pond that exceeds that which is consistent with that change in pressure, i.e. $\frac{\partial P_{pond}}{\partial P} < -1$. In this case the feedback has infinite gain (Roe 2009). Pond growth rate is limited by the balance between insolation and the latent heat of melting ($O(10^3)$ yr for melting of a 1km-thick ice sheet, Earthlike insolation, $\alpha = 0.6$, and 10% of sunlight going to melting), or by thermal diffusion of heat into a stratified pond. For tectonic activity levels that are not too high, the SDF is much faster than the ESWI, which is limited by volcanic degassing rates and tectonic resurfacing rates (0.05 mm/yr on Earth (Leeder 1999); 16 mm/yr on Io (Rathbun et al. 2004)). The SDF stops when insolation is insufficient to allow further pond growth. What happens after the SDF has operated will depend on the sign of the carbonate-silicate feedback at the new, modifed P. If $\partial W_t/\partial P > 0$, the normal carbonate-silicate feedback will rejuvenate the atmosphere on a volcanic degassing timescale, freezing the ocean. If $\partial W_t/\partial P < 0$, pressure decreases further.

Gases that react chemically with seawater (such as SO_2 and CO_2; Zeebe & Wolf-Gladrow (2001)) can have P_{pond} much greater than that given by Henry's law. For example, total Dissolved Inorganic Carbon (DIC, $\propto P_{pond}$) is buffered against changes in P by carbonate chemistry, and P_{pond} changes much more slowly than Henry's law. $P_{pond} \propto P^{0.1}$ for the modern Earth ocean, as opposed to $P_{pond} \propto P$ for Henry's law (Zeebe & Wolf-Gladrow 2001; Goodwin et al. 2009). For a decrease in P that increases ψ_{max}, this buffering favors the tendency of increasing pond volume to draw down more atmosphere, against the Henry's Law decrease in atmospheric concentration per unit pond. Carbonate buffering is less important for $P >\sim$1 bar, because at the correspondingly low pH the DIC partitions almost entirely into CO_2. For CO_2, we use R. Zeebe's scripts (`http://www.soest.hawaii.edu/oceanography/faculty/zeebe_files/CO2_System_in_Seawater`

/csys.html) to find the additional DIC held in the ocean as HCO_3^- and CO_3^{2-}. We use fixed alkalinity, 2400 μmol/kg (similar to the present Earth ocean; Zeebe & Wolf-Gladrow (2001)). Figure 6 shows the results. ψ_{max} is set by Equation 1 through $T_s(\psi)$. Ocean circulation adds additional heat transport terms to Equation 1, which we ignore. We also do not consider buffering by dissolution and precipitation of carbonates or salts (such as sulfates).

As an example of SDF, consider the partitioning of an initial 1-bar total inventory of CO_2 (blue-green contour labelled '0' in Figure 6) with increasing L_*. Initially, the planet's surface is below freezing. As stellar flux is increased to 800 W/m^2, a small sea forms and dissolves some of the CO_2. The system is within the area where SDF is a positive feedback on small changes in P (outermost black contour in Figure 6), which accelerates sea growth. A small further increase in L_* leads to runaway SDF (innermost black contour in Figure 6), and ocean area quickly grows with from ∼5% to ∼15% of planet surface area with no change in L_*. After this change the atmospheric inventory is reduced to 1/4 bar with the remaining 3/4 bar dissolved in the ocean. Further pond growth requires further increase in L_*. Increasing T_{pond} decreases solubility and shallows the slope of increasing volatile inventory stored in the ocean. By $L_* = 3800$ W/m^2 (the highest considered), the ocean covers almost the entire lightside hemisphere, and stores ∼5/6 of the initial CO_2 inventory. Further small increases in L_* cause a global ocean.

Three main effects control this system:- (1) Cosine fall-off of starlight weakens the ability of decreasing pressure to increase ocean area beyond a relatively small ψ_{max}. Following a line of decreasing pressure, the dashed red lines (fractional ocean area) become more widely spaced with decreasing pressure. Cosine falloff of stellar radiation is responsible. This restricts the scope of the instability, which tends to lead to Eyeball states (Pierrehumbert 2011). We do not find any cases where the SDF can turn a dry planet into an ocean-covered planet or vice versa. (2) Ocean instability disappears above ∼5 bars, when the surface is nearly isothermal. Because decreases in pressure always decrease $\bar{T}_s$ (except when there is an antigreenhouse), decreases in pressure can only cause oceans to freeze over. Below ∼5 bars, ΔT_s is not negligible. If a decrease in pressure allows the substellar temperature to rise above freezing, an ocean can form. (3) Rectification of starlight by the terminator, and of ocean area by the melting point, divides the phase diagram into 'no ocean', 'substellar ocean' and 'global ocean' zones. On the nightside T_s is constant, so ocean area jumps from 50% to 100%. Notice the change in sign of L_* dependence below and above the dashed red line corresponding to 50% ocean area. In the substellar ocean zone, increasing L_* increases ocean area and the ocean inventory increases. However, in the global ocean zone, increasing L_* cannot increase ocean area. The decrease in gas solubility with increasing temperature dominates, and the ocean inventory decreases.

Figure 6 does show unstable regions in parameter space for which substellar dissolution is a positive feedback on changes in P (solid black lines). These always correspond to small oceans (<10% of planet surface area). But the gain of the feedback is small, and runaways cannot occur unless ocean depth >10km. Factor–of–3 decreases (or increases) in atmospheric pressure can occur with no change in the total (atmosphere + ocean) inventory of volatile substance. The SDF is a

minor positive feedback (or a negative feedback) for most gases which dissolve simply according to Henry's Law. The buffering effect is not sufficient to allow ocean area to give a strong positive feedback. Finally, $\Lambda = 0.03$ is unrealistically low for all-CO_2 atmospheres. Setting $\Lambda = 1$ would shut down the instability. We conclude that the CO_2 SDF is unlikely to be important for planets in synchronous rotation, and is important in fewer cases than is the ice-albedo feedback (Roe & Baker 2010; Pierrehumbert et al. 2011).

5. Discussion

5.1. Solar system climate stability - is Mars a solar system example of ESWI?

Although ESWI is most relevant for planets in synchronous rotation, it can work for any planet with sufficiently high ΔT_s. Therefore, in order to test ESWI against available data, we compare the requirements for ESWI to Solar System data (Table 1). After correcting for the distorting effects of life, all of the Solar System's non-giant atmospheres are overwhelmingly one gas. Except for Earth, the principal gas is also the main greenhouse gas. Venus' atmospheric composition is not controlled by the abundance of surface liquid (nor in solid-state equilibrium with surface minerals; Hashimoto & Abe (2005); Tremain & Bullock (in press)), and Triton's atmosphere is too thin to stabilize liquid nitrogen. Climate regulation on Titan is not well understood. Currently, the greenhouse effect of CH_4 outcompetes the antigreenhouse effect of the organic haze layer (McKay et al. 1991). The production rate of the organic haze layer depends on $[CH_4]$ (McKay et al. 1991; Lorenz et al. 1997). ESWI is not currently possible on Titan because ΔT_s is too small, 2.5-3.5K (Jennings et al. 2009). Therefore, out of 5 nearby worlds with atmospheres and surfaces, only Mars is a candidate for ESWI (§5.1). Solar System data suggest that the conditions for the ESWI are quite restrictive, and that most planets will not be susceptible to the ESWI.

Mars may have passed through ESWI in the past. The main climate-controlling greenhouse gas (CO_2) can dissolve in liquid water and be sequestered as carbonate minerals. Mars has low P (95% CO_2). It has widespread deposits of carbonate minerals (Bandfield et al. 2003; Wray et al. 2011), but little or no surface liquid water. It currently sits at the gas-liquid sublimation boundary (Kahn 1985), with $\Delta T_s \sim$100K , and GCMs show that $\Delta T_s \downarrow$ as $P \uparrow$ (Richardson & Mischna 2005). These geologic and climatic observations are all consistent with a past rapid transition via ESWI from an early thicker atmosphere to the current state, as follows. Increasing solar luminosity could have permitted transient liquid water, allowing carbonate formation. The corresponding drawdown in P would increase noontime temperature, allowing a further increase in liquid water availability and the rate of carbonate formation. The runaway would slow as P approached the triple-point buffer: loss of liquid water stability may have throttled weathering and buffered the climate near the triple point (Kahn 1985; Halevy et al. 2007). However, ice is not ubiquitous on the surface and can migrate away from warm spots, so unusual orbital conditions are neccessary for melting

(Kite et al. 2011a,b). Alongside carbonate formation, atmospheric escape, polar cold trapping and volcanic degassing are the four main processes affecting P on Mars over the last 3 Ga. However, recent volcanism has been sluggish and probably CO_2-poor (Hirschmann & Withers 2008; Werner 2009; Stanley et al. in press), and present-day atmospheric escape appears slow (Barabash et al. 2007). Polar cold traps hold ∼1 Mars atmosphere of CO_2 as ice today (Phillips et al. 2011), but this trapping should be reversable at high obliquity. Therefore, it is quite possible that substellar (≡ noontime) carbonate formation has been the dominant flux affecting the secular evolution of Mars' atmosphere since 3.0 Gya. This hypothesis deserves further investigation.

5.2. Application to exoplanets

5.2.1. How general is our feedback?

ESWI requires:

– *Strong temperature dependence of the weathering drawdown of greenhouse gases.* Decreasing k_{ACT} to 0.03 (from the nominal 0.09) eliminates the ESWI except for radiatively inert atmospheric compositions. On the other hand, increasing k_{ACT} to 0.27 causes a large unstable region even for $\Lambda = 1.0$, with at least a 1 dex range of atmospheric pressure unstable to ESWI for all habitable-zone luminosities.

Earth data on the value of k_{ACT} are consistent with $k_{ACT} \sim 0.1$. However, deep-time calibration of weathering-temperature relations such as Equation 3 is difficult. There is only one planet (Earth) to use as laboratory, with constantly drifting boundary conditions, and rather few natural experiments. Chemical weathering rates of silicate minerals in the lab are definitely temperature-dependent (White & Brantley 1995), but erosion-rate dependence is also important at the scale of river catchments (West et al. 2005). Confirming temperature dependence on geological scales is difficult, in part because today's weathering rate contains echoes of glacial-interglacial cycles (Vance et al. 2009). Regression of present-day river loads on watershed climatology by West et al. (2005) suggests an e-folding temperature of 8.5(+5.5/-2.9)K. $^{187}Os/^{188}Os$ data suggest continental weathering rates increased 4-8x in $\ll 10^6$ yr during a Jurassic hyperthermal ($\Delta T \leq 10$K) 0.183 Gya (Cohen et al. 2004), implying an e-folding temperature <(5 – 7)K. Analysis of the apparent time dependence of weathering rate gives support to a hydrological control on weathering rates (Maher 2010), but on a planetary scale precipitation always increases when T_s increases (O'Gorman & Schneider 2008). That is, $\frac{DW}{Dt} = \frac{\partial W}{\partial T_s} + \frac{\partial W}{\partial R}\frac{\partial R}{\partial T_s}$ with $\frac{\partial R}{\partial T_s} > 0$.

Overall, Equation 3 is consistent with deep-time, present-epoch, and laboratory estimates for Earth. Though Equation 3 is used in this paper as a general rule for Earth-like planets, the weathering-temperature relation is shaped by biological innovations. For example, the symbiosis between vascular plants and root fungi (arbuscular mycorrhizae) acidifies soil, profoundly accelerates weathering, and may be unique to Earth (Taylor et al. 2009). All geologically important

surface weathering reactions require a liquid phase (White & Brantley 1995). We assume weathering reactions do continue below the freezing point (due to microclimates, or monolayers of water). However, the results shown in Figure 4 and 5 did not change qualitatively when we set $W = 0$ for $T < T_{melt}$.

Strong temperature dependence could break down in several ways. For example, erosion is needed to expose fresh mineral surfaces for weathering. On a tectonically quiescent planet (and for tectonically quiescent regions of an active planet) weathering may be limited by supply of fresh surfaces, with weathering going to completion on all exposed silicate minerals. On tectonically very active planets with little or no land, hydrothermal alteration and rapid seafloor spreading maintain low greenhouse gas levels with little or no temperature dependence (Sleep & Zahnle 2001). A planet with weathering rates that are limited by the availability of liquid water (like Mars) can have effectively temperature-dependent weathering, but only if the atmospheric pressure is well above that fluid's triple point.

– *Large* ΔT_s. The high-ΔT_s requirement cannot be met if the atmosphere is thick. A deep global ocean circulation behaves like a thick atmosphere - Earth abyssal temperatures vary <2K from tropics to poles (Schlitzer 2000). Therefore, the climate destabilization mechanism cannot operate on a planet with a deep global ocean circulation - at least some land is necessary. Evaporation will dry out land at the substellar point if $\bar{T}_s$ is high, so weathering activity may be concentrated at cooler ψ in this case. ΔT_s varies little, or even increases, with rotation frequency (Merlis & Schneider 2010; Edson et al. 2011). Therefore, ESWI could work for rapidly-rotating planets such as Mars (§5.1). However, the isothermal approximation does not apply when the Coriolis force prevents fast equator-to-pole winds. For rapid rotators, T_s is a function of latitude and longitude, and our idealized energy balance model is not appropriate.

– *Small* Λ. Strong greenhouse gases have high Λ, which suppresses ESWI. On the other hand, Λ can be negative if there is an antigreenhouse effect ($\Lambda < 0$). M-dwarfs later than M4, with fully convective interiors, seem to remain active with high UV fluxes for much longer than do Sunlike stars. High UV fluxes broadly favor CH_4 accumulation (Segura et al. 2005) and perhaps antigreenhouse haze effects. When $\Lambda < 0$, ESWI will apply for all P and L_*.

– *Surface-atmosphere coupling.* This consists of radiative and turbulent coupling. Turbulent coupling requires a nonzero near-surface wind speed, and that the global near-surface atmosphere is not stably stratified. A sensitivity test with a 10–fold reduction in U showed that the pressure range unstable to ESWI moves to $\sim 10\times$ higher pressure. The range of Λ subject to ESWI was significantly reduced. We assume U is not a function of P, but simulations show that U increases as P decreases (Melinda A. Kahre, via email). This would strengthen the instability.

SDF has very similar requirements to ESWI, but the constraint on rotation rate is stricter. Large-amplitude libration or nonsynchronous rotation would prevent the development of a deep pond around the substellar point. (A low-latitude liquid belt can be imagined, but the idealized EBM of §2 is not appropriate to that case). Kepler data show that only a small proportion of close-

in small-radius exoplanets in multi-planet systems are in mean-motion resonance (Lissauer et al. 2011), but that most are close to resonance and could maintain nonzero eccentricity. This would allow for significant nonsynchronous rotation if the planet's spin rate adjusts to keep the substellar point aligned with the star during periapse passage (pseudo-synchronous rotation). In addition, SDF requires very soluble gases: by contrast, the N_2 content of even a 100km deep ocean at 298K is only ∼0.2 bar per bar of atmospheric N_2. In this paper we assume that volatiles are excluded from the ice when the ice freezes. If clathrate phases form, they could absorb volatiles and make the SDF irreversible.

5.2.2. Climate evolution into the unstable region

Planets could undergo ESWI early in their history if they form in the unstable region. In addition, many common geodynamic and astronomical processes can shift the equilibrium between W_t and V_n (Figure 4a), causing a secular drift of the equilibrium across the phase space $\{L_*, \Lambda, V_t\}$ (Figures 3 and 5). This drift can take a planet from a stable equilibrium to an unstable equilibrium via a saddle-node bifurcation (Strogatz et al. 1994).

• *Dynamics and stellar evolution:* Theory predicts that the secular increase in solar flux should have gradually shifted the position of Earth's climate equilibrium. This is consistent with the sedimentary record of the last 2.5 x 10^9 yr (Grotzinger & Kasting 1993; Grotzinger & James 2000; Ridgwell & Zeebe 2005; Kah & Riding 2007). For Kepler field (Sunlike, rapidly evolving) stars, this could also occur and potentially cause the ESWI for planets with initially thick atmospheres (Figure 4a). For M stars, main-sequence insolation changes little over the lifetime of the Universe.

• *Atmospheric evolution:* Λ can change as atmospheric composition evolves. For example, the rise in atmospheric oxygen following the emergence of oxygenic photosynthesisers probably oxidized atmospheric CH_4 and may have caused a catastrophic decline in Λ (Kopp et al. 2005; Domagal-Goldman et al. 2008). Even gases with negligible opacity, such as N_2, alter Λ through pressure broadening (Li et al. 2009). Carbonate-silicate weathering equilibrium is impossible for planets where atmospheric erosion exceeds geological degassing. For these planets, V_n is negative. Strong stellar winds and high XUV flux are observed for many M stars. Removal of atmosphere by strong stellar winds (Mura et al. 2011) or, for smaller planets, high XUV flux (Tian 2009) could trigger an instability for a planet orbiting an M-star, by reducing P (Figure 4a).

• *Tectonics and volcanism:* Volcanic activity decays with radioactivity (Kite et al. 2009; Sleep 2000, 2007; Stevenson 2003), so in the absence of tidal heating the equilibrium pressure will gradually fall (on a stable branch where W_t increases with P) (Figure 4a). Superimposed on this decline are pulses in volcanic activity due to mantle plumes, and perhaps planetwide volcanic overturns as seem to have occurred on Venus. This will cause spikes in equilibrium pressure. The rate of resurfacing is very sensitive to mantle composition, tidal heating, and tectonic style (Kite et al. 2009; Valencia & O'Connell 2009; Korenaga 2010; Běhounková et al. 2010, 2011; van Summeren et

al. 2011). Shutdown of volcanism (such that $V_n \leq 0$) extinguishes the possibility of a stable climate equilibrium; P will fall monotonically. ESWI can accelerate this decay, and Mars may be an example of this (§5.1). Mountain range uplift exposes fresh rock and may provide a $O(10^7)$ yr increase in weathering rate that cools the planet (as arguably and controversially may have occurred for Tibet, Earth: Garzione (2008)). This may trigger ESWI by lowering pressure. More speculatively, drift of continents can cause very large atmospheric pressure fluctuations if greenhouse-gas drawdown occurs mainly on land and is strongly focussed in a high-weathering patch near $\psi = 0$. A continent drifting over the patch will increase planet-averaged weatherability, and pressure will go down.

6. Summary and conclusions

Nearby M-dwarfs are targeted by several planet searches:- MEarth (Charbonneau et al. 2009); the VLT+UVES M-dwarf planet search (Zechmeister et al. 2009); the VLT+CRIRES M-dwarf planet search (Bean et al. 2010); HARPS (Forveille et al. 2011); M2K (Apps et al. 2010); and proposed space missions TESS (Deming 2009); ELEKTRA; PLATO; and ExoplanetSat (Smith et al. 2010). These searches are driven in part by the hope that planets orbiting M-dwarves can maintain surface liquid water and be habitable. Maintaining surface liquid water over geological time involves equilibrium between greenhouse-gas supply and removal. Balance is thought to be maintained on habitable planets through temperature-dependent weathering reactions. Climate stability can be undermined by several previously-studied climate instabilities. These include atmospheric collapses (Haberle et al. 1994; Read & Lewis 2004), photochemical collapses (Zahnle et al. 2008; Lorenz et al. 1997), greenhouse runaways (Kasting 1988; Lorenz et al. 1999; Sugiyama et al. 2002), ice-albedo feedback (Roe & Baker 2010), and ocean thermohaline circulation bistability (Stommel 1961; EPICA Community Members 2006). Climate stability can also be undermined if the sign of the dependence of mean surface weathering rate on mean surface temperature is reversed. This paper identifies two new climate instabilities that involve such a reversal, and are particularly relevant for planets orbiting M-dwarves.

Competition between radiative and advective heat transfer timescales sets surface temperature on synchronously-rotating planets with an atmosphere. The atmosphere moves the surface temperature towards the planetary average, through radiative and turbulent heat exchange, on timescale t_{dyn}. The dayside insolation gradient acts to reestablish gradients in surface temperature, on timescale t_{rad}. We refer to planets with $t_{dyn} < t_{rad}$ as dynamically equilibrated, because surface temperature is set by atmospheric dynamics. Venus and Titan are nearby examples. We refer to planets where $t_{dyn} \geq t_{rad}$ as radiatively equilibrated. Mars is a nearby example.

Steeper horizontal temperature gradients promote atmospheric depletion if they stabilize surface liquid films, ponds or oceans in which the atmosphere can dissolve. Once dissolved, the atmospheric gases may be sequestered in the crust by weathering. Weathering rates are much faster when solvents are present and temperatures are high. Weathering and mineral formation can be mediated by thin films of water, and are largely irreversible on habitable-zone planets with

stagnant lid geodynamics (karst and oceanic dissolution layers are minor exceptions). Lithospheric recycling may cause metamorphic decomposition of weathering products, returning greenhouse gases to the atmosphere on tectonic timescales. In the absence of weathering, growth of an ocean can reduce atmospheric pressure through dissolution. For example, the fundamental greenhouse gas on Earth is CO_2. The partitioning of CO_2 between the atmosphere, ocean (solution) and crust (weathering products) is in the ratio $1{:}50{:}10^5$ for Earth (Sundquist & Visser 2007). Dissolution is fully reversible. Positive feedback occurs if reduced atmospheric pressure further steepens the temperature gradient. Rising maximum temperature resulting from atmosphere drawdown allow further expansion of liquid stability, leading to more drawdown. The zone where liquid is stable spreads over the substellar hemisphere. A halt to the atmospheric collapse occurs when pressure approaches the boiling curve, or when the liquid phase is stable over most of the dayside, or when thermal decomposition by crustal recycling returns weathering products to the atmosphere as fast as they are produced.

Our idealized-model results motivate study of the instabilities with GCMs.

We conclude from this study that:-

1. Enhanced substellar weathering instability (ESWI) may destabilize climate on some habitable-zone planets. ESWI requires large ΔT_s, which is most likely on planets in synchronous rotation. ESWI does not require strict 1:1 synchronous rotation.

2. Substellar dissolution feedback (SDF) is less likely to destabilize climate. It is only possible for restrictive conditions: small oceans, highly soluble gases, and relatively thin, radiatively weak atmospheres. Furthermore, small amounts of nonsynchronous rotation can eliminate SDF.

3. The proposed instabilities only work when most of the greenhouse forcing is associated with a weak greenhouse gas that also forms the majority of the atmosphere (it does not work for Earth). There are no exact solar system analogs to ESWI, although Mars comes close. Therefore, it would be incorrect to use these tentative results to argue against prioritizing M-dwarfs for transiting rocky planet searches.

4. If the ESWI is widespread, we would expect to see a bimodal distribution of day-night temperature contrasts and thermal emission from habitable-zone rocky planets in synchronous rotation. Rocky planets with surface pressures in the unstable region would be rare, so emission temperatures would be either close to isothermal, or close to radiative equilibrium.

Acknowledgements. Itay Halevy collaborated with E.S.K. on the development of this idea for Mars (§5.1). We thank Itay Halevy, Ray Pierrehumbert, Rebecca Carey, Dorian Abbott, and especially Ian Eisenman for productive suggestions. Robin Wordsworth and Francois Forget shared output from their exoplanet GCM. E.S.K. thanks Dan Rothman for stoking E.S.K.'s interest in deep time

climate stability. E.S.K. and M.M. acknowledge support from NASA grants NNX08AN13G and NNX09AN18G. E.G. is supported by NASA grant NNX10AI90G.

REFERENCES

Apps, K., et al., PASP, 122, 156.

Bahcall, J. N., Pinsonneault, M. H., & Basu, S. 2001, ApJ, 555, 990.

Bandfield, J.L., Glotch, T.D., & Christensen, P.R. 2003, Science 301, 1084.

Barabash, S., Federov, A., Lundin, R., & Sauvaud, J.-A. 2007, Science 315, 501.

Batalha, N.M. & the Kepler Team 2011, ApJ 729, 2011.

Bean, J. L., Seifahrt, A., Hartman, H., et al. 2010, ApJ, 713, 410

Běhounková, M., et al. 2010, J. Geophys. Res. - Planets 115(E9), CiteID E09011.

Běhounková, M., et al. 2011, ApJ 728, 89.

Berner, R.A., & Z. Kothavala 2001, Am. J. Sci. 301, 182.

Charbonneau, D., et al. 2009, Nature 462, 891.

Cohen, A.S., Coe, A.L., Harding, S.M., & Schwark, L. Geology 32, 157.

Cowan, N.B., & Agol, E. 2011, ApJ 729, 54.

Deming, D. et al. 2009, PASP 121, 952.

Deming, D., & Seager, S. 2009, Nature 462, 301.

Domagal-Goldman, S.D., Kasting, J.F., Johnston, D.T., & Farquhar, J. 2008, Earth Planet. Sci. Lett. 269, 29.

Edmond, J.M., & Huh, Y. 2003, Earth Planet. Sci. Lett. 216, 125.

Edson, A., Lee, S., Bannon, P., Kasting, J.F., & Pollard, D. 2011, Icarus 212, 1.

EPICA Community Members (first author C. Barbante) 2006, Nature 444, 195.

Lawson, P.R., Traub, W.A. & Unwin, S.C. 2009, Exoplanet Community Report, Jet Propulsion Laboratory Publication 09–3.

Forveille, T., Bonfils, X., Lo Curto, G., et al. 2011, A&A, 526, A141

Garzione, C.N. 2008, Geology 36, 1003.

602 Goodwin, P., et al. 2009, Nat. Geosci. 2, 145.

603 Grotzinger, J.P., & James, N.P. 2000, p. 3-20 in Grotzinger, J.P. & James, N.P. (Eds). Carbonate
604 Sedimentation and Diagenesis in the Evolving Precambrian World, SEPM Sp. Pub. 67,
605 Tulsa, OK.

606 Grotzinger, J.P., & Kasting, J.F. 1993, J. Geol. 101, 235.

607 Haberle, R.M., Tyler, D., McKay, C.P., & Zahnle, K.J. 1994, Icarus 109, 102.

608 Halevy, I., Zuber, M.T. & Schrag, D.P. 2007, Science 318, 1903.

609 Hashimoto, G.L., & Abe Y. 2005, Planet. & Space Sci. 53, 839.

610 Hirschmann, M.M., & Withers, A.C. 2009, Earth Planet. Sci. Lett. 270, 147.

611 Jackson, B., et al. 2010, Mon. Not. R. Astron. Soc. 407, 910.

612 Jennings, D.E. et al. 2009, ApJL 691, L103-L105.

613 Joshi, M.M., Haberle, R.M., & Reynolds, R.T. 1997, Icarus 129, 450.

614 Joshi, M. 2003, Astrobiology 3, 415.

615 Kah, L.C., & Riding, R. 2007, Geology 35, 799.

616 Kahn, R. 1985, Icarus 62, 175.

617 Kasting, J.F. 1988, Icarus 74, 472.

618 Kasting, J.F. 1991, Icarus 94, 1.

619 Kasting, J.F., Whitmire, D.P., & Reynolds, R.T. 1993, Icarus 101, 108.

620 Kite, E.S., Manga, M., & Gaidos, E. 2009, ApJ 700, 732.

621 Kite, E.S., Michaels, T.I., Rafkin, S.C.R., Manga, M., & Dietrich, W.E. 2011a, J. Geophys. Res.
622 116, E07002, doi:10.1029/2010JE003783.

623 Kite, E.S., Rafkin, S.C.R., Michaels, T.I., Dietrich, W.E., & Manga, M. 2011b, J. Geophys. Res.,
624 doi:10.1029/2010JE003792, in press.

625 Knutson, H., Charbonneau, D., Cowan, N. B., Fortney, J. J., Showman, A. P., Agol, E., Henry,
626 G.W., Everett, M.E., & Allen, L.E., ApJ 690, 822.

627 Kopp, R. E., Kirschvink, J. L., Hilburn, I. A., & Nash, C. Z. 2005, Proceedings of the National
628 Academy of Science, 1021, 11131.

629 Korenaga, J. 2010, ApJL 725, L43.

630 Kump, L.R., Brantley, S.L., & Arthur, M.A. 2000, Ann. Rev. Earth Planet. Sci. 28, 611.

631 Leeder, M.R. 1999, Sedimentology and sedimentary basins: from turbulence to tectonics (1st Edi-
632 tion), Wiley-Blackwell.

633 Léger, A., & the CoRoT Team 2009, A&A 506, 287.

634 Lissauer, J. J., Ragozzine, D., Fabrycky, D. C., et al. 2011, arXiv:1102.0543.

635 Li, K.-F., Pahlevan, K., Kirschvink, J. L., & Yung, Y. L. 2009, Proceedings of the National Academy
636 of Science, 106, 9576.

637 Liu, J., & Schneider, T. 2011, J. Atmos Sci., in press.

638 Lorenz, R.D., McKay, C.P., & Lunine, J.I. 1997, Science 275, 642.

639 Lorenz, R.D., McKay, C.P., & Lunine, J.I. 1999, Plan. and Space Sci. 47, 1503.

640 Maher, K. 2010, Earth Planet. Sci. Lett. 294, 101.

641 Marinova, M., McKay, C.P., & Hashimoto, H. 2005, J. Geophys. Res. 110, E03002,
642 doi:10.1029/2004JE002306.

643 Matsui, T. & Abe, Y. 1986, Nature 319, 303

644 McKay, C.P., Pollack, J.B., & Courtin, R. 1991, Science 253, 1118.

645 Merlis, T.M., & T. Schneider 2010, Journal of Advances in Modeling Earth Systems 2, 13,
646 doi:10.3894/JAMES.2010.2.13

647 Mitchell, J.L., & Vallis, G.K. 2010, J. Geophys. Res. 115, E12008, doi:10.1029/2010JE003587.

648 Morbidelli, A., Tsiganis, K., Crida, A., Levison, H.F., & Gomes, R. 2007, AJ 134, 1790.

649 Mura, A., et al. 2011, Icarus 211, 1.

650 Murray, C.D., & Dermott, S.F. 1999, Solar System Dynamics, Cambridge.

651 Murphy, B.A., Farley, K.H., & Zachos, J.C. 2010, Geochem. Cosmochem. Acta 74, 5098.

652 O'Gorman, P.A., & Schneider, T., 2008, J. Climate 21, 3815.

653 Phillips, R.J., et al. 2011, Science 332, 838.

654 Pielke, R.A. 2002, Mesoscale Meteorological Modeling, International Geophysics Series 78, Aca-
655 demic Press.

656 Pierrehumbert, R.T. 1995, J. Atmos. Sci. 52, 1784.

657 Pierrehumbert, R.T. 2002, Nature 419, 191.

Pierrehumbert, R.T. 2010, Principles of Planetary Climate, Cambridge University Press.

Pierrehumbert, R.T. 2011, ApJL 726, L8.

Pierrehumbert, R.T., & Gaidos, E. 2011, ApJL 734, L13.

Pierrehumbert, R.T., Abbot, D.S, Voigt, A., & Koll, D. 2011, Ann. Rev. Earth Planet Sci. 39, 417.

Rathbun, J.A., Spencer, J.R., Tamppari, L.K., Martin,T.Z., Barnard, L. & Travis, L.D. 2004, Icarus 169, 127.

Read, P.L., & Lewis, S.R. 2004, The Martian climate revisited: atmosphere and environment of a desert planet, Springer-Praxis.

Richardson, M.A., & Mischna, M.I. 2005, J. Geophys. Res. 110, E03003, doi:10.1029/2004JE002367.

Ridgwell, A., & Zeebe, R.E. 2005, Earth Planet. Sci. Lett. 234, 299.

Roe, G. 2009, Ann. Rev. Earth Planet. Sci. 37, 93.

Roe, G.H., & Baker, M.B. 2010, J. Climate 23, 4694.

Sander, R. 1999, Compilation of Henry's Law Constants for Inorganic and Organic Species of Potential Importance in Environmental Chemistry (Version 3) http://www.henrys-law.org

Schlitzer, R. 2000, Eos. Trans. AGU 81(5), 45 (`ewoce.org`).

Schneider, T., O'Gorman, P. A., & Levine, X. J. 2010, Reviews of Geophysics, 48, 3001

Segura, A., et al. 2005, Astrobiology 5(6),706.

Selsis, F., Wordsworth, R., & Forget, F. 2011, A&A accepted, doi:10.1051/0004-6361/201116654.

Sleep, N.H. 2000, J. Geophys. Res., 105, 17563

Sleep, N.H. 2007, ch.9.06 in Treatise on Geophysics, Elsevier.

Sleep, N. H., & Zahnle, K. 2001, J. Geophys. Res., 106, 1373.

Smith, M.W. 2010, Proc. SPIE 7731, 773127 (2010); doi:10.1117/12.856559

Showman, A.P., Cho, J. Y-K., & Menou, K. 2010, Atmospheric Circulation of Exoplanets, in Seager, S. (Ed)., Exoplanets, U. Arizona Press.

Stanley, B.D., Hirschmann, M.M., & Withers, A.C., Geochim. et Cosmochimica Acta, in press, doi:10.1016/j.gca.2011.07.027.

Strogatz, S.H. 1994, Nonlinear dynamics and chaos, Perseus Books.

Stevenson, D.J. 2003, Comptes Rendus de l'Acadamie, 335, 99.

686 Stommel, H. 1961, Tellus 13, 224.

687 Sugiyama, M., Stone, P.H., & Emanuel, K.A. 2002, J. Atmos. Sci. 61, 2001.

688 Sundquist, E.T., & Visser K. 2007, Treatise on Geochemistry, Chapter 8.09, 425-472.

689 Tarter, J.C., Backus, P.R., Mancinelli, R.L., Aurnou, J.M., et al. 2007, Astrobiology 7, 3065.

690 Taylor, L.L., et al. 2009, Geobiology 7, 171.

691 Tian, F. 2009, ApJ 703, 905.

692 Tremain, A.H., & Bullock, M.A., Icarus, in press, doi:10.1016/j.icarus.2011.08.019

693 Valencia, D., & O'Connell, R.J. 2009, Earth Planet. Sci. Lett. 286, 492.

694 Vance, D., Teagle, D.A.H., & Foster, G.L. 2009, Nature 458, 493.

695 van Summeren, J., Conrad, C.P., & Gaidos, E., ApJL 736, L15.

696 Walker, J.C.G , Hays, P.B., & Kasting J.F 1981, J. Geophys. Res. 86, 1147.

697 Werner, S.C. 2009, Icarus 201, 44.

698 West, A.J., Galy, A., & Bickle, M. 2005, Earth Planet. Sci. Lett. 235, 211.

699 White, A.F., & Brantley, S.L. 1995, Chemical weathering rates of silicate minerals, Rev. Mineral.,
700 v31, Min. Soc. Am.

701 Winn, J.N., et al. 2011, ApJL 737, L18.

702 Wordsworth, R.D., arXiv:1106.1411v1 [astro-ph.EP]

703 Wordsworth, R.D., Forget, F., Selsis, F., Millour, E., Charnay, B., & Madeleine, J.-B. 2011, ApJ
704 733, L48.

705 Wray, J.J., et al. 2011, 42nd Lunar and Planetary Science Conference, held March 711, 2011 at
706 The Woodlands, Texas. LPI Contribution No. 1608, p.2635

707 Zahnle, K., Haberle, R.M., Catling, D.C., & Kasting, J.F. 2008, J. Geophys. Res. 113, E11004.

708 Zechmeister, M., Kürster, M., & Endl, M. 2009, A&A, 505, 859.

709 Zeebe, R.E., & Wolf-Gladrow, D. 2001, CO_2 in seawater: equilibrium, kinetics, isotopes, Elsevier
710 Oceanography Series, v.65.

711 Zeebe, R.E., & Caldeira, K. 2008, Nature Geoscience 1, 312, doi:10.1038/ngeo18.

712 Zeebe, R.E, Zachos, J.C. & Dickens, G.R. 2009, Nature Geoscience 2, doi: 10.1038/ngeo578.

This preprint was prepared with the AAS LaTeX macros v5.2.

Table 1. Solar system climates, showing vulnerability to ESWI and SDF.

Planet	Atmospheric composition	Climate-controlling GHG	Requirements: (1)	(2)	(3)	(4)
Venus	97% CO_2	CO_2	√	√	×	×
Earth	99% N_2 (a)	CO_2	×	√	√	×
Mars	**95% CO_2**	**CO_2**	**√**	**√**	**√/?**	**√**
Titan	98% N_2	N_2 or H_2/CH_4 (b)	(√)	√	√	√
Triton	> 99.9% N_2	n.a.	√	×	×	n.a. (c)

Note. —Requirements for the instability include: (1) The principal gas in the atmosphere is the main climate-controlling greenhouse gas. (2) The atmosphere significantly influences surface temperature. (3) Removal of gas by liquid phase, *via* weathering or dissolution, is an important loss mechanism. (4) $\bar{T} < T_{melt} < \max(T_s)$.

(a) Earth: Ignoring oxygen, which is an artefact of biology. (b) Titan: Small fractional or absolute changes in $[N_2]$ have the largest effect on Titan's τ (Lorenz et al. 1999). However, this ignores vapor-pressure and photochemical feedbacks which may put $[H_2]$ in control (McKay et al. 1991). (c) Triton: Surface melting is impossible, because N_2's triple point is $10^4\times$ greater than Triton's surface pressure.

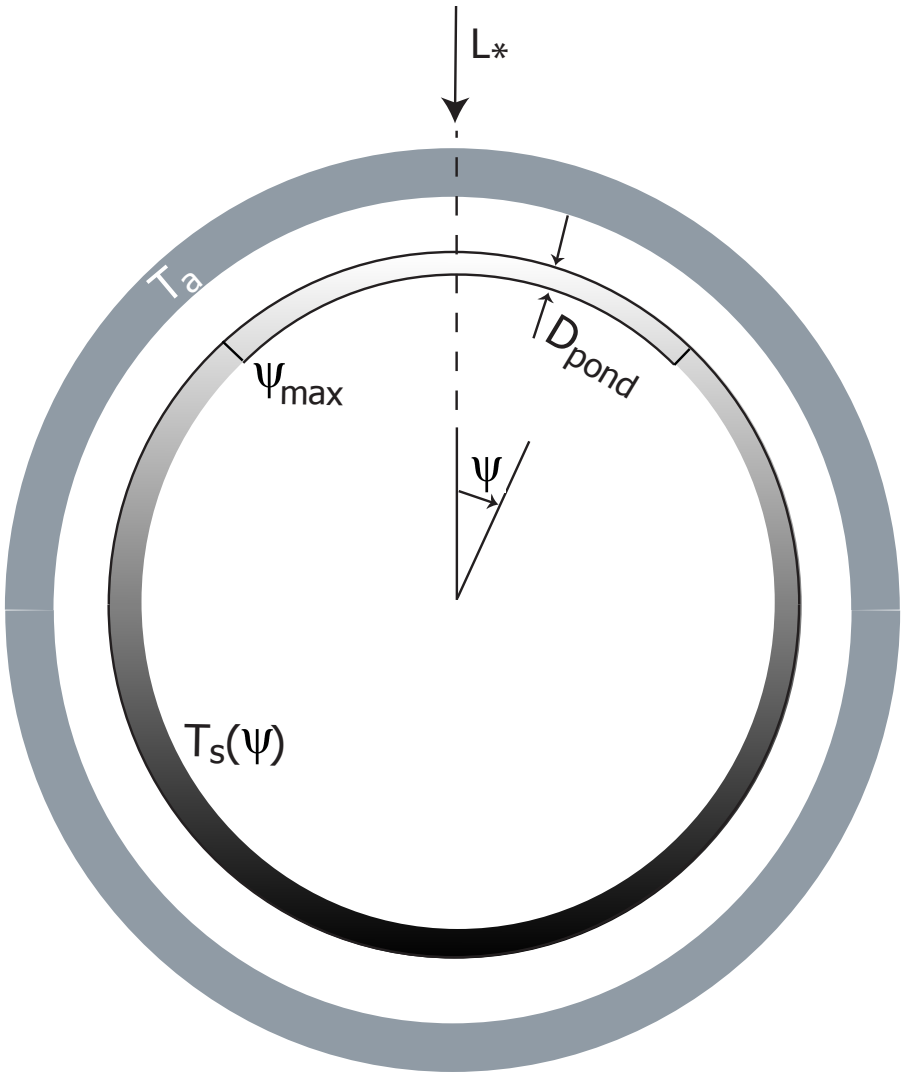

Fig. 1.— Geometry of the idealized energy balance model for an exoplanet in 1:1 spin-orbit resonance. Uneven distribution of starlight (L_*) on the planet leads to a hot (white shading, high T_s) dayside surface and a cool (black shading, low T_s) nightside surface. The atmosphere (uniform gray shading), with horizontally uniform boundary-layer temperature T_a, tends to reduce this temperature gradient (ΔT_s). When $T_s > T_{melt}$, a melt pond can form around the substellar point $\psi = 0$, with angular radius ψ_{max} and depth D_{pond}. Because rotation is slow, meridional winds are as fast as zonal winds, so T_s depends only on the angular distance from the substellar point (ψ).

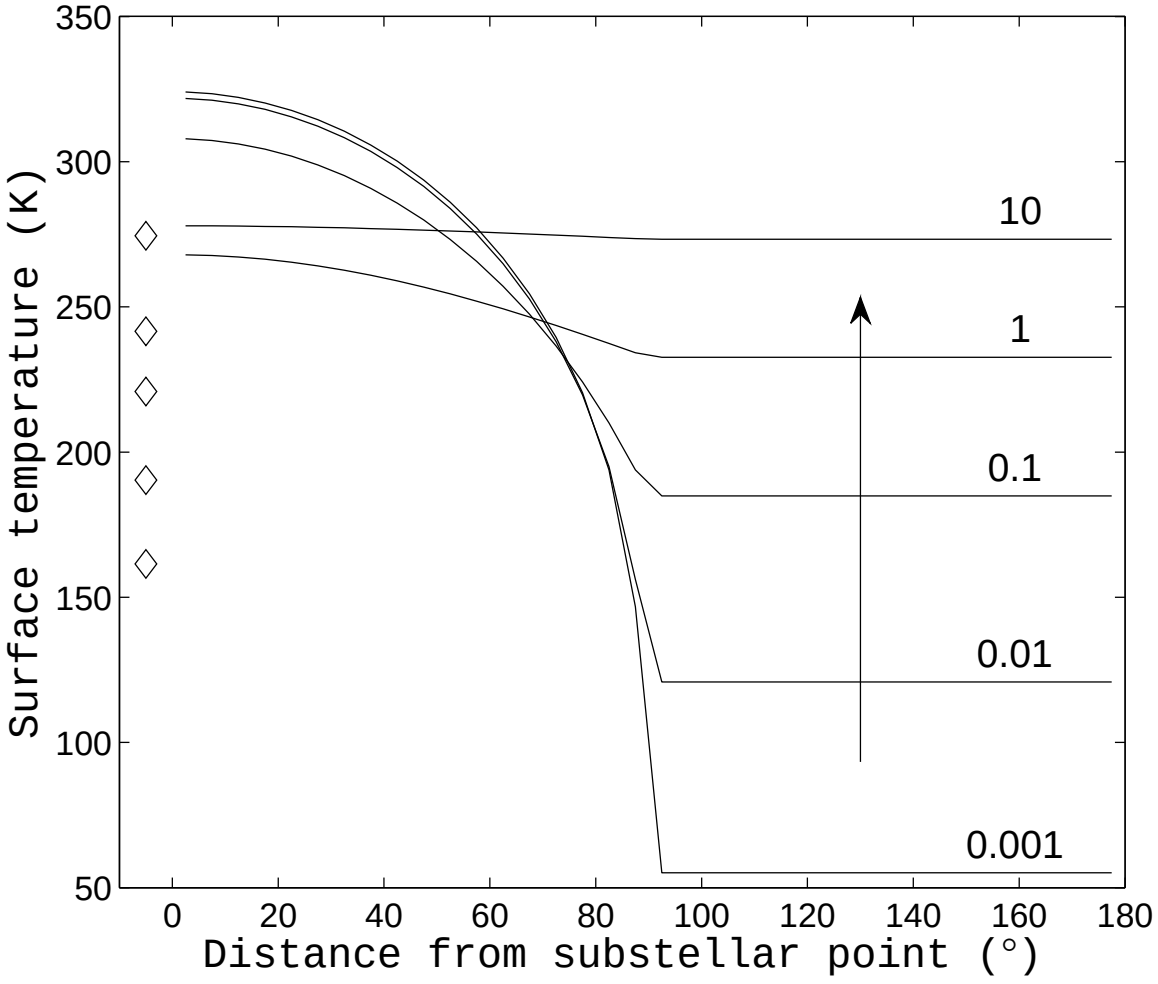

Fig. 2.— Surface temperature as a function of distance from the substellar point in our energy balance model. Diamonds correspond to atmospheric temperature (horizontally uniform). In order of increasing temperature, the pressures corresponding to the diamonds are 10^{-3}, 10^{-2}, 10^{-1}, 1 and 10 bars. Arrow is the direction of increasing pressure. Radiative efficiency $\Lambda = 0.1$, stellar flux $L_* = 900$ W/m^2.

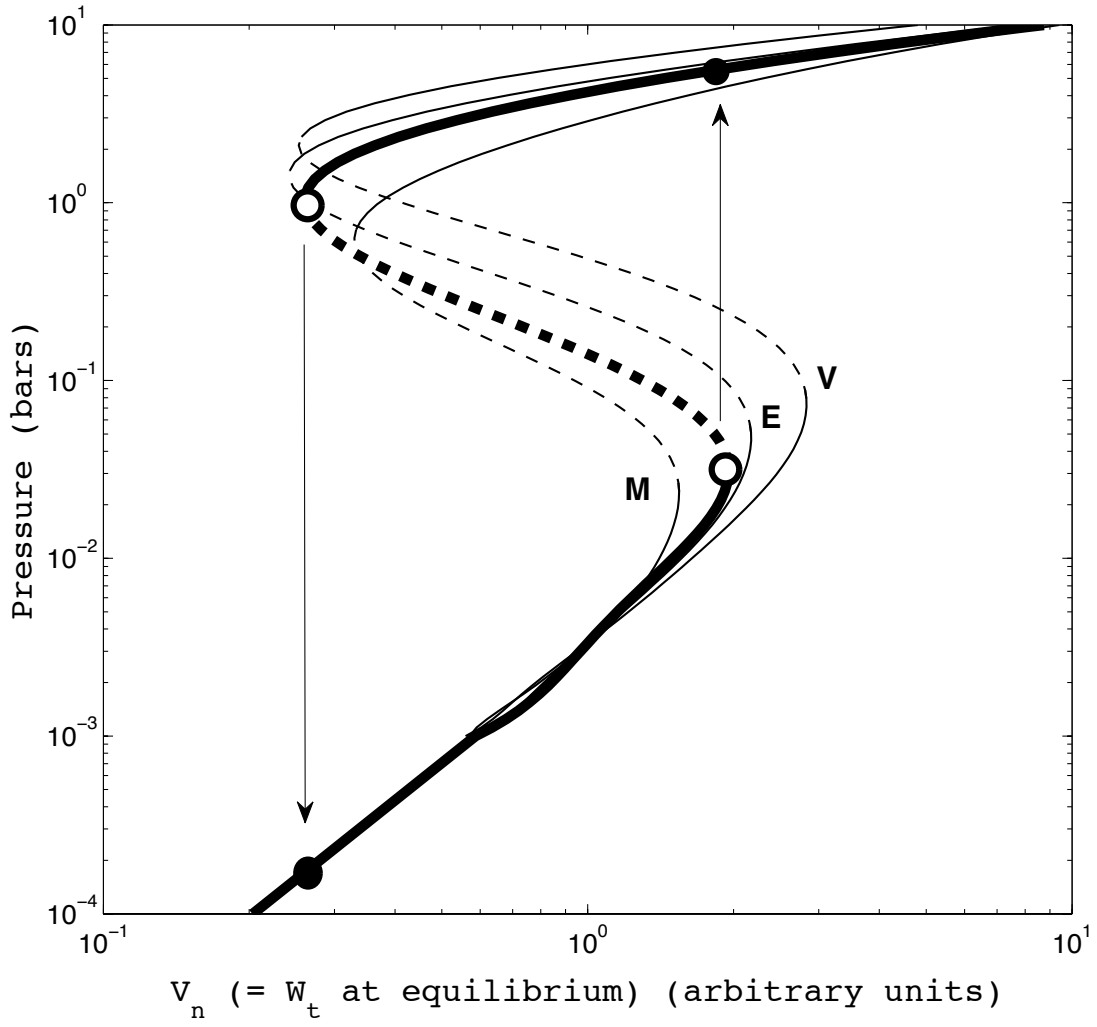

Fig. 3.— Bifurcation diagram to show the enhanced substellar weathering instability for radiative efficiency $\Lambda = 0.1$, stellar flux $L_* = 900$ W/m^2. The thick black line shows the planet-integrated weathering, W_t, corresponding to the temperature maps shown in Figure 2. If $V_n = 0$, $W_t \propto -\left(\frac{\partial P}{\partial t}\right)$. $\frac{\partial P}{\partial t} = 0$ at equilibrium, and W_t equals net supply by other processes, V_n. For both the lowest and highest P, $W_t\uparrow$ as $P\uparrow$. Equilibria on these branches are stable. For intermediate pressures, $W_t\downarrow$ as $P\uparrow$. The thick dashed line is this unstable branch. The rapid climate transitions which bound the hysteresis loop are shown by vertical arrows. The corresponding unstable equilibria are shown by open circles, and stable equilibria are shown by closed circles. The thin black lines correspond to Mars, Earth and Venus insolation (in order of increasing normalized weathering rate). The shape of the curve is explained in the text. These curves are an 8th-order polynomial fit to the model output. Note that as $L_*\uparrow$, both inflection points move to higher P.

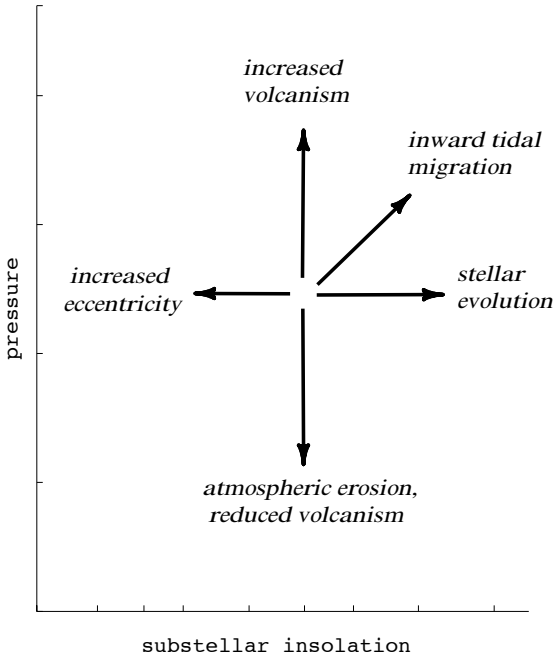
increased volcanism
inward tidal migration
increased eccentricity
stellar evolution
atmospheric erosion, reduced volcanism
pressure
substellar insolation

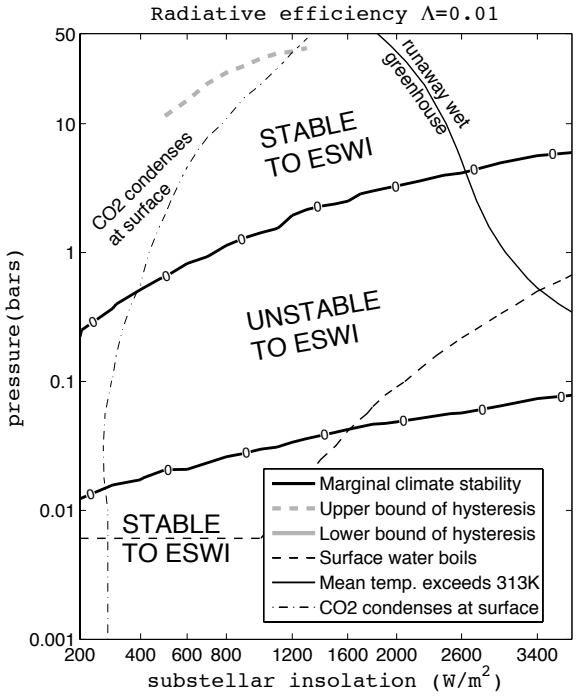
Radiative efficiency Λ=0.01
runaway wet greenhouse
CO2 condenses at surface
STABLE TO ESWI
UNSTABLE TO ESWI
STABLE TO ESWI
Marginal climate stability
Upper bound of hysteresis
Lower bound of hysteresis
Surface water boils
Mean temp. exceeds 313K
CO2 condenses at surface
pressure(bars)
substellar insolation (W/m2)

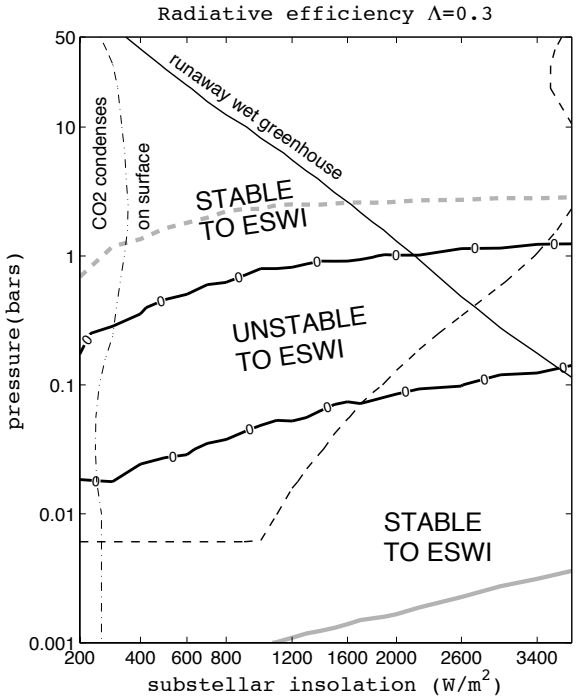
Radiative efficiency Λ=0.3
runaway wet greenhouse
CO2 condenses on surface
STABLE TO ESWI
UNSTABLE TO ESWI
STABLE TO ESWI
pressure(bars)
substellar insolation (W/m2)

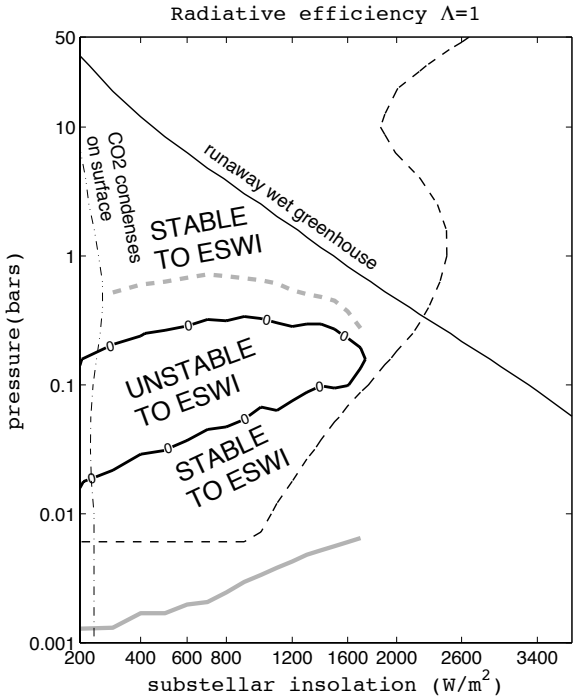
Radiative efficiency Λ=1
runaway wet greenhouse
CO2 condenses on surface
STABLE TO ESWI
UNSTABLE TO ESWI
STABLE TO ESWI
pressure(bars)
substellar insolation (W/m2)

Fig. 4.— (a) Mechanisms that can cause secular change in the location of the climate equilibrium $W_t = V_n$. (b,c,d) Habitable zone (HZ) stability diagrams for (b) $\Lambda = 0.01$, (c) $\Lambda = 0.3$, (d) $\Lambda = 1.0$. (Climates with $\Lambda >> 1$ are always stable against the enhanced substellar weathering instability). The climate states at intermediate pressure within the thick black line labelled with zeros are unstable to ESWI $\left(\frac{\partial W_t}{\partial P} < 0\right)$. Climates that approach the unstable zone from below will jump up to the dashed gray line. Climates that approach the unstable zone from above will jump down to the solid gray line. These jumps can be extreme; for example, in (b) the solid gray line is everywhere < 0.001 bars (and so is not visible). See the text for discussion of the speed of jumps. The hysteresis loop does not exist for high L_* and and high Λ, and so the thick gray lines vanish towards the right of (d). The thin lines correspond to previously-described challenges to habitable-zone climate stability: moist runaway greenhouse (thin solid line); nightside atmospheric condensation of CO_2 (dash-dotted line); boiling of surface water (thin dashed line).

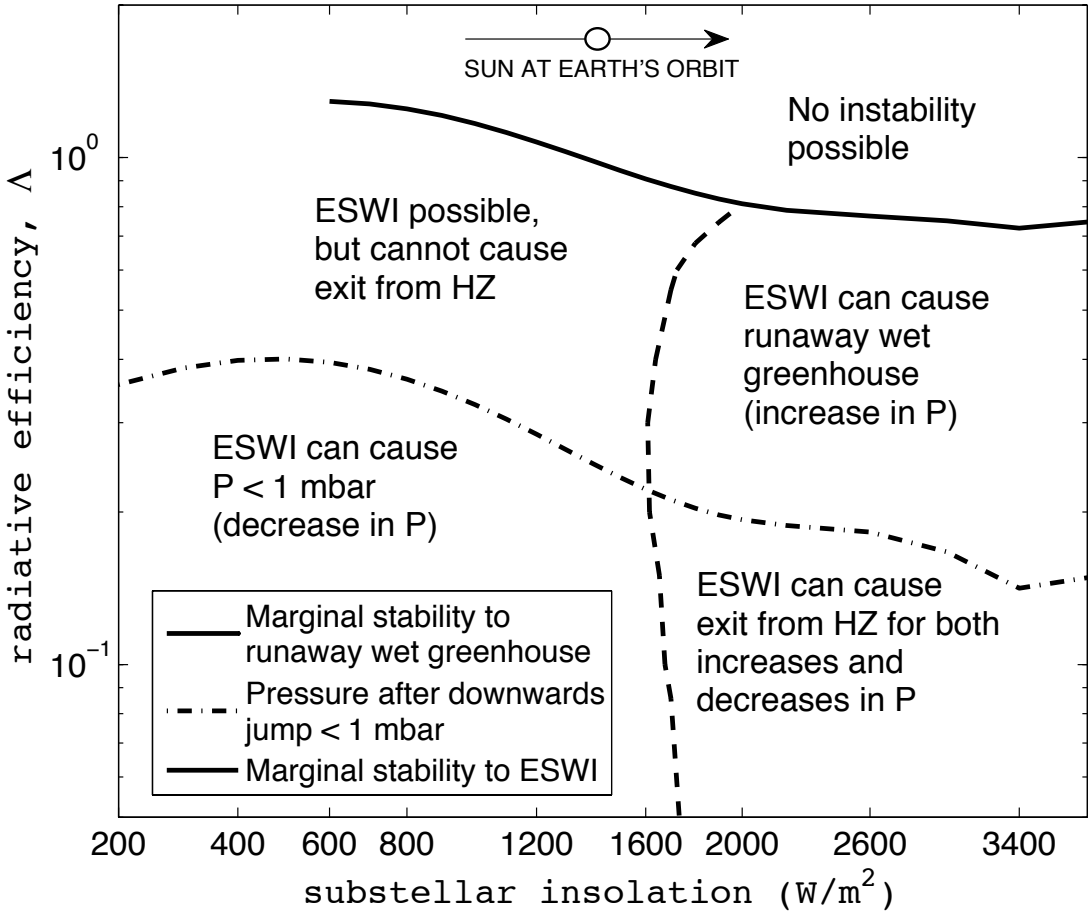

Fig. 5.— Stability phase diagram, showing the effects of the enhanced substellar weathering instability as a function of L_* and Λ. The jump in pressure due to ESWI can cause a runaway wet greenhouse (for a jump upwards in P), or a decrease in P to the triple point of water (for a jump downwards in P). To account for microclimates and solid-state greenhouse effects, we conservatively define "$P <$ triple point" as "$P < 1$ mbar", which is below the boiling curves in Figure 4. Some curves have been smoothed with a 5th-order polynomial in order to remove small wiggles due to numerical artifacts. The arrow shows the change in stellar flux at 1AU for a solar-mass star over 8 Gyr of stellar evolution in the model of Bahcall et al. (2001), and the circle marks the current solar flux.

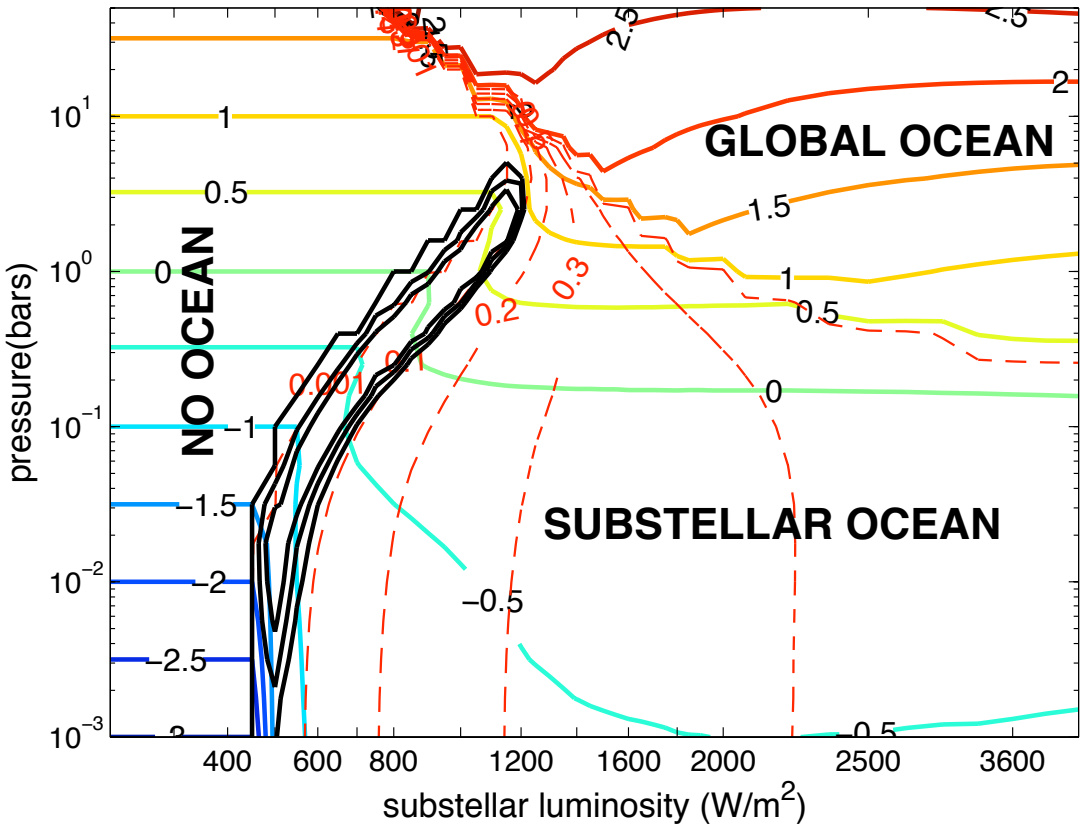

Fig. 6.— Substellar dissolution feedback, for CO_2/seawater equilibria, $\Lambda = 0.03$ (note that $\Lambda = 0.03$ is unrealistically low for all-CO_2 atmospheres), and a 100km-deep ocean. The vertical axis is P. Colored solid lines correspond to log10($P + P_{pond}$), i.e. the sum of the atmospheric and ocean inventory. Where these are equal to P, there is no ocean. Fractional ocean coverage is shown by the red dashed contours (contour interval is 0.1 in units of planet fractional surface area). Because nightside temperature is constant, fractional ocean coverage jumps from 0.5 (hemispheric ocean) to 1.0 (global ocean). The outermost black line encloses the area where SDF is a positive feedback on small changes in P. Outside this area, $\frac{\partial P_{pond}}{\partial P} \geq 0$ (zero or negative climate feedback). The inner two contours correspond to $\frac{\partial P_{pond}}{\partial P} <$ -0.5 (strong positive feedback) and $\frac{\partial P_{pond}}{\partial P} <$ -1 (runaway). Runaways can only occur for deep oceans and small pond area.